Theoretical Chemistry Accounts (2024) 143:45
https://doi.org/10.1007/s00214-024-03120-1

RESEARCH

Mechanistic investigation on the gas-phase thermal decomposition of triazene-bridged nitro-1,2,4-triazole

Congming Ma[1] · Kehan Hu[1] · Peng Ma[1] · Wenxin Xia[1]

Received: 11 March 2024 / Accepted: 26 April 2024 / Published online: 18 May 2024

Abstract

Electronic structure methods based on quantum mechanics were employed to characterize elementary steps for the gas-phase thermal decomposition of triazene-bridged nitro-1,2,4-triazole (**TBBT**). Homolytic *C*–NO_2 bond scission and ·NO_2 elimination were the most energetically favorable unimolecular paths for the initial decomposition. From there, sequences of unimolecular reactions for daughters of the initiation steps through low-energy β-scission reactions and ring-opening reaction were postulated and characterized. Hydron shift, C–N bond breakage, nitrogen and NO_2 elimination, and small molecules like CN–N=NH obtained were all characterized. Creating a comprehensive network that can be used to develop a detailed limited rate chemical dynamic mechanism for simulating decomposition of **TBBT**, the results provide the foundation for **TBBT**'s combustion modeling, and response to its aging, and storage.

Keywords Decomposition mechanism · Energetic compounds · Nitro-1,2,4-triazole · Triazene-bridged · Density functional theory

1 Introduction

Compared to traditional energetic materials, modern nitrogen-rich energetic compounds have the advantages of high gas production, high heat of formation, and high density due to their abundant C–N, N–N, and N=N bonds [1–3]. They have become potential candidates for high-energy insensitive explosives, smokeless pyrotechnic agents, solid fuels for propellants, and gas generators. Azole compounds have become one of the basic skeletons of energetic compounds due to their high nitrogen content. Among them, the planar structure of 1,2,4-triazole precursors has low ring tension and high molecular stability, making them widely favored by energetic material researchers. The structural diversity of monocyclic triazole compounds is limited, and the introduction of energetic groups to increase energy comes at the cost of reduced molecular stability and increased sensitivity. Therefore, the strategy of connecting two or more triazole rings through connecting groups to construct bridging triazole energetic compounds is one of the effective strategies for constructing new energetic compounds. Compared with carbon bridges, nitrogen-bridged triazole energetic compounds endow energetic molecules with higher nitrogen content, thereby increasing the heat of formation of the compounds, and forming larger conjugated systems, promoting the dense accumulation of crystals, increasing molecular stability, and thus reducing sensitivity.

Klapötke et al. [4] successfully synthesized triazene-bridged bis(methyltetrazolyl)triazenes (**A** and **B**) using methyl-5-aminotetrazole as one raw material, which displays poor detonation performance. Later, Pang et al. [5] synthesized a novel triazene-bridged methyl-1,2,3-triazole (**C**), showing similar properties comparing to methyl-5-aminotetrazole series. Recently, Wu et al. [6, 7] designed and synthesized triazene-bridged nitro-1,2,4-triazole (**TBBT**) successfully, which revealed excellent detonation properties (Fig. 1). Various physical properties of solid-state **TBBT** have been characterized. It was observed that its decomposition temperature was relatively low of 154.6 °C using differential scanning calorimetry (DSC), and impact sensitivity was 45 J. In order to build finite-rate chemical kinetics mechanism, explore reasons for a low decomposition point, the electronic structure methods based on quantum mechanics were used to characterize the potential energy landscape

✉ Peng Ma
mpcctv@163.com

[1] College of Safety Science and Engineering, Nanjing Tech University, Nanjing 211816, China

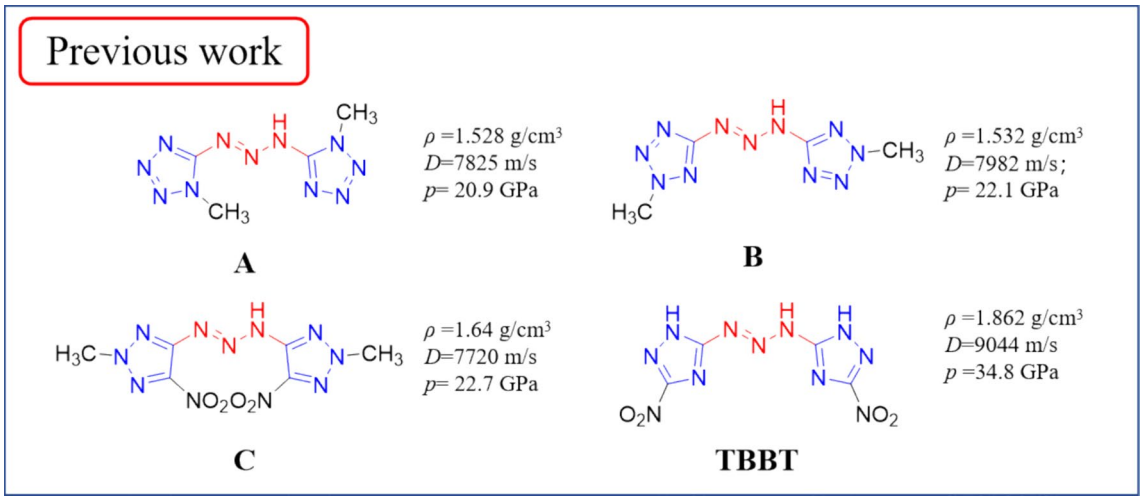

Fig. 1 Representative triazene-bridged energetic compounds

of **TBBT**'s thermal decomposition as a follow-up theoretical research. Key results are reported and discussed.

2 Computational methods

Geometry optimizations were performed with Gaussian 16 software package [8]. All isomers and transition state (TS) structures related to triazene-bridged nitro-1,2,4-triazole were obtained using the M06-2× functional and the 6-311g(*d*,*p*) basis set at 298.15 K and 1 atm. Besides, bond order analysis was performed using Multiwfn software [9–11]. When considered necessary, intrinsic reaction coordinate (IRC) was performed to verify whether the transition state structure connects reactants and products as expected. To obtain more accurate relative energies for the critical points, the aug-cc-pVDZ basis set was employed to obtain refined single-point electronic energies for them [12].

3 Results and discussion

3.1 Decomposition landscape of TBBT

A large number of reactions with potential relevance to **TBBT**'s gas-phase decomposition were considered, and energetically favored unimolecular steps were presented in Scheme 1. It seems that decomposition of **TBBT** undergoes homolytic *C*–NO_2 bond scission and ·NO_2 elimination in the initial step, followed by two possible decomposition steps after ring-opening. Among them, **INT21** generates **INT81** eventually through hydrogen transfer, N–C cleavage, generation of N_2, N–C cleavage, and generation of ·NO_2 and ·CN; **INT32** generates nitroacetonitrile through nitrogen removing, N–C and N–N cleavage; and **INT24** also generates nitroacetonitrile through removing a long nitrogen chains, along with a simultaneous breakage of N–C and N–N bonds. The most favorable decomposition steps are indicated by red arrows, and details of these pathways, as well as those of less favorable routes, are discussed in the following subsections.

3.2 Comparison of initial unimolecular decomposition steps

As for triazene-bridged nitro-1,2,4-triazole (**TBBT**), the results of Laplace bond order analysis (Table 1) indicated that both *C*–NO_2 and N–H bonds have smaller bond orders, indicating their relative low stability. Thus, the potential for all preliminary bond breaks in **TBBT** is shown in Fig. 2, including homolytic scission of the N–H (R11, R12, and R13) and *C*–NO_2 (R14 and R15) bonds. The former reaction of R11 was found to be 374.76 kJ/mol endothermic, 574.02 kJ/mol for R12, and 556.97 kJ/mol for R13. The latter reactions of R14 or R15 were found to be nearly 290 kJ/mol endothermic, which would be competitive with the former reactions and might be a possible reason for its relatively lower decomposition point. No transition states occured in the above reactions. Consequently, it is unlikely that a direct ring-opening reaction did not occur during the initial decomposition process, but the substituent attached to the triazole rings seems to be more prone to breakage, obtaining the triazole-functionalized radical **INT14** with initial NO_2 loss.

Considering that N–H and *C*–NO_2 bonds are more prone to breakage (Table 1), two reaction pathways were performed, leading to **INT22** and **INT23** with a barrier of 291.51 kJ/mol and 375.26 kJ/mol, respectively. Besides,

Scheme 1 Energetically favored unimolecular decomposition steps

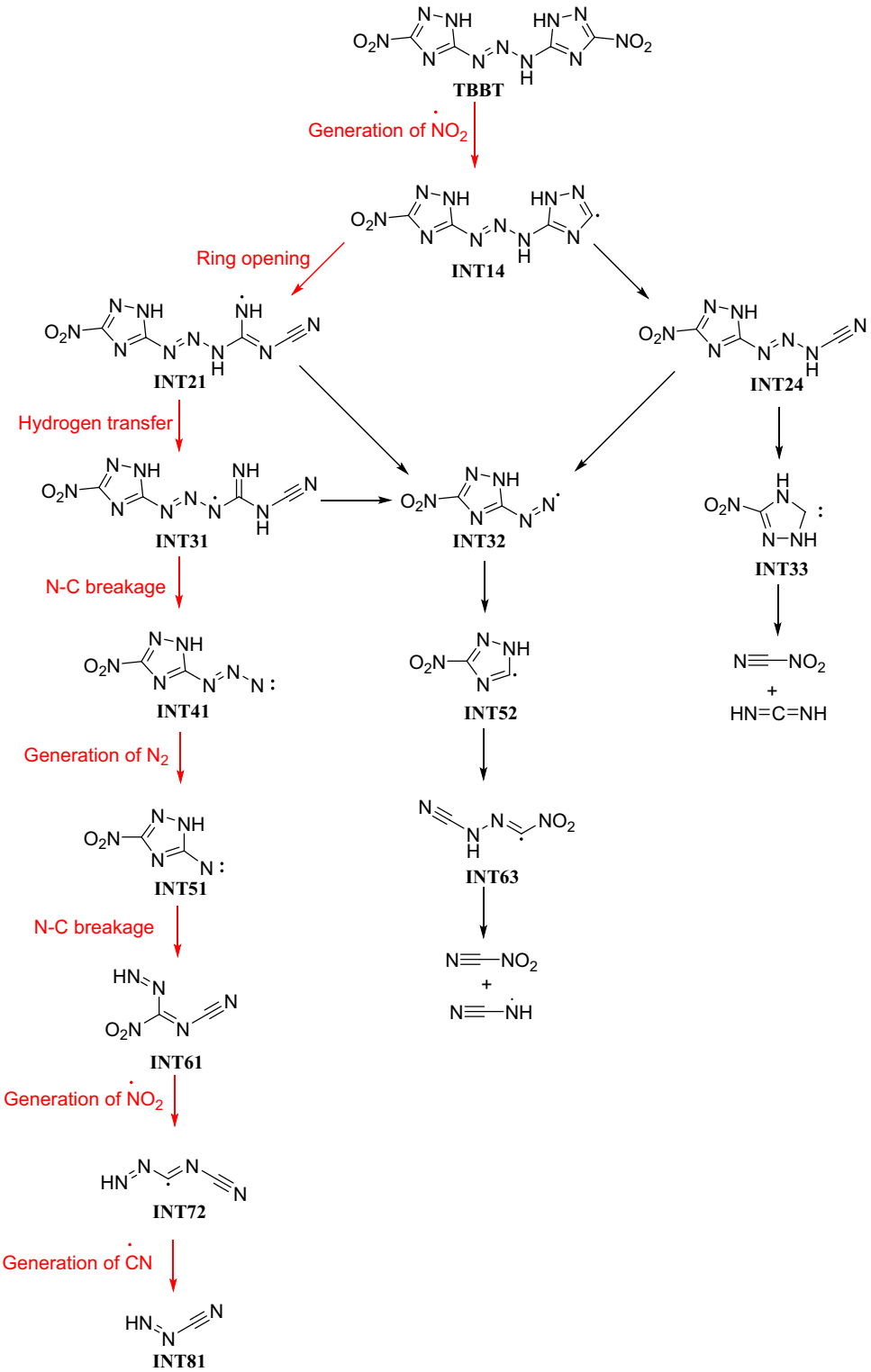

Table 1 Laplace bond order analysis of **TBBT**

Bond	LBO	Bond	LBO	Bond	LBO
N8–H21	0.651026	N1–N5	0.882842	C11–N10	1.093266
N5–H20	0.679647	N7–N8	0.940612	N14–O16	1.095238
N13–H22	0.685267	C9–N8	0.997760	N14–O15	1.095554
C11–N17	0.754229	C4–N6	1.005280	N17–O19	1.096395
C2–N14	0.759461	C4–N5	1.036272	N17–O18	1.098152
N12–N13	0.793979	C9–N13	1.055711	C2–N3	1.141364
N1–N5	0.895848	C4–N5	1.084777	N6–N7	1.377788

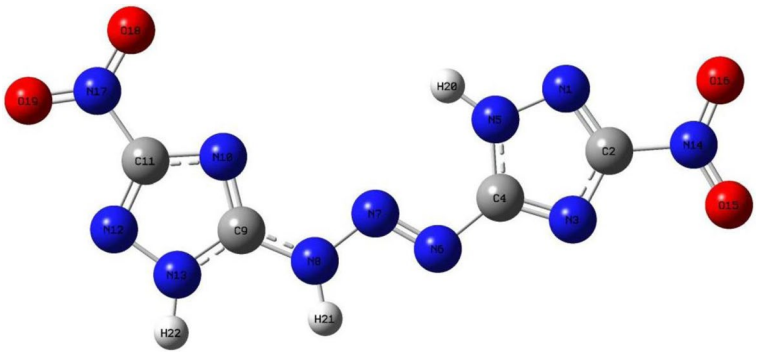

low-energy β-scission reactions were possible to occur, radical **INT14** was postulated to decompose via the cleavage of C–N (R24) or N–N (R21) bond. The barrier for R24 was found to be 288 kJ/mol, and the reaction was 173.17 kJ/mol endothermic (see Fig. 3). However, unlike R24, which produces a closed-shell intermediate (**INT24**) through the cleavage of two C–N bonds of the triazole ring (**TS24**), R21 undergoes a separate N–N bond cleavage, with formation of a transition state **TS21** and generation of a cyano group eventually (see Fig. 3). The barrier necessary to open **INT14**'s radical-containing ring (via R21) was found to be 108 kJ/mol and produced another radical (**INT21**), with 56.51 kJ/mol exothermic. It is concluded that products with two free radical sites are more difficult to form, and reactions are more likely to occur when the breakage of the original chemical bond is conducive to formation of a new one by free radicals.

Based on the above results for **TBBT**'s unimolecular decomposition steps, **INT21** and **INT24** were postulated to be the two most critical intermediates, and further exploration of the decomposition mechanism was then discussed.

3.3 Decomposition path of INT21

3.3.1 Initial decomposition of INT21

According to the resonance theory, the secondary amine radical (**INT21**) can form a resonance isomer with the adjacent enamine structure, and the obtained single nitrogen atom radical (**INT21a**) would be more stable due to the electron-withdrawing effect of the cyano group (see Fig. 4). To our surprise, a reaction involving the hydrogen transfer process from **INT21a** to **INT31** occurred, whose barrier to form **TS31** was found to be 170.91 kJ/mol, and the reaction was fairly exothermic.

Additionally, **INT21** can further fall apart to **INT32** and HNC(NH)NCN with the barrier of 215.80 kJ/mol, and the reaction was 169.55 kJ/mol endothermic. This reaction was driven by two secondary amine radicals connected to the C8 atom (see Fig. 5), which formed a new chemical bond with double-bond property, thereby stabilizing the two single nitrogen radical. At the same time, the bonding electrons of the enamine bond and the cyano group are shifted, and finally, the structure of carbodiimide was formed (see Fig. 6).

3.3.2 Unimolecular decomposition of INT31

The triazole ring of **INT31** is connected with nitro group and a long chain of seven atoms. Considering the instability of the triazene structure, the intermediates **INT32** and **INT41** can be obtained by breaking C–N bond and N–N bond, respectively. **INT32** was produced with the barrier of 291.14 kJ/mol, and the reaction was 195.29 kJ/mol endothermic (see Fig. 7), which has a barrier of 75 kJ/mol higher than that of R32, suggesting that it is not easy to obtain radical azo structures. Another intermediate **INT41** is a triazene structure with nitrogen lone pair electrons. As shown in Fig. 7, the barrier of R41 was strongly lower than that of

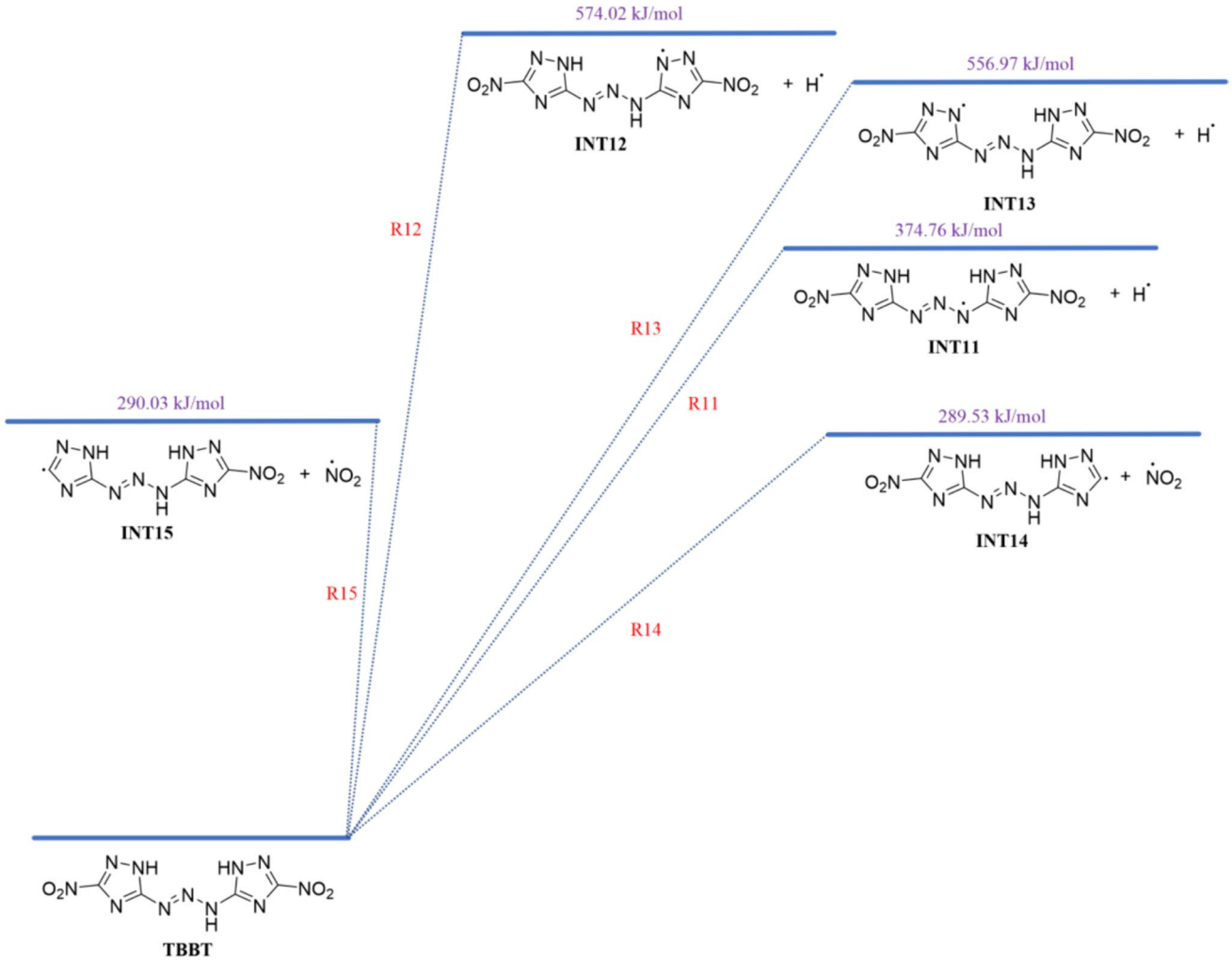

Fig. 2 Decomposition of **TBBT** initiation reactions. All energy profiles (kJ/mol) show the relative Gibbs free energy with the energy of the initial reactant as zero

R42 (84.44 kJ/mol vs. 291.14 kJ/mol). Therefore, it would likely prove to be the favored route.

3.3.3 Unimolecular decomposition of INT41

Firstly, attempts to break C4–N6 bond of **INT41** were considered, producing an unstable N_3 structure. Thus, a more reasonable unimolecular decomposion step was postulated via the loss of stable nitrogen. The barrier of R51 was found to be 171.21 kJ/mol, and the reaction was 32.69 kJ/mol endothermic (see Fig. 8).

The barrier necessary to open **INT51**'s ring (via R62) was found to be 195.54 kJ/mol. The effect of lone pair electrons in the nitrogen atom was considered in this decomposition process, which forms a cyanide group and another nitrogen atom with lone pair electrons while breaking the C1=N3 double bond of the triazole ring. Then, the C2–N4 bond undergoes homocleavage and forms a double bond between C2 and N3, ultimately resulting in **INT62**.

The most stable closed-shell intermediate formed by R61 was **INT61**, which was generated through R61 process, with cleavage of C1–N9 bond in the triazole ring firstly and formation free radicals separately. Subsequently, the C2–N4 bond was ruptured, forming N4=N9 and C2=N3 double bonds simultaneously. R61 has a barrier of 145.86 kJ/mol, and the reaction was 5.82 kJ/mol endothermic. This suggests that ring-opening of the triazole is the preferred decomposition route.

3.3.4 Unimolecular decomposition of INT61

INT61 is a closed-shell molecule produced by **INT51**. Postulating R71–R73 as a sequence of possible unimolecular steps for its composition, as expected for the homolytic

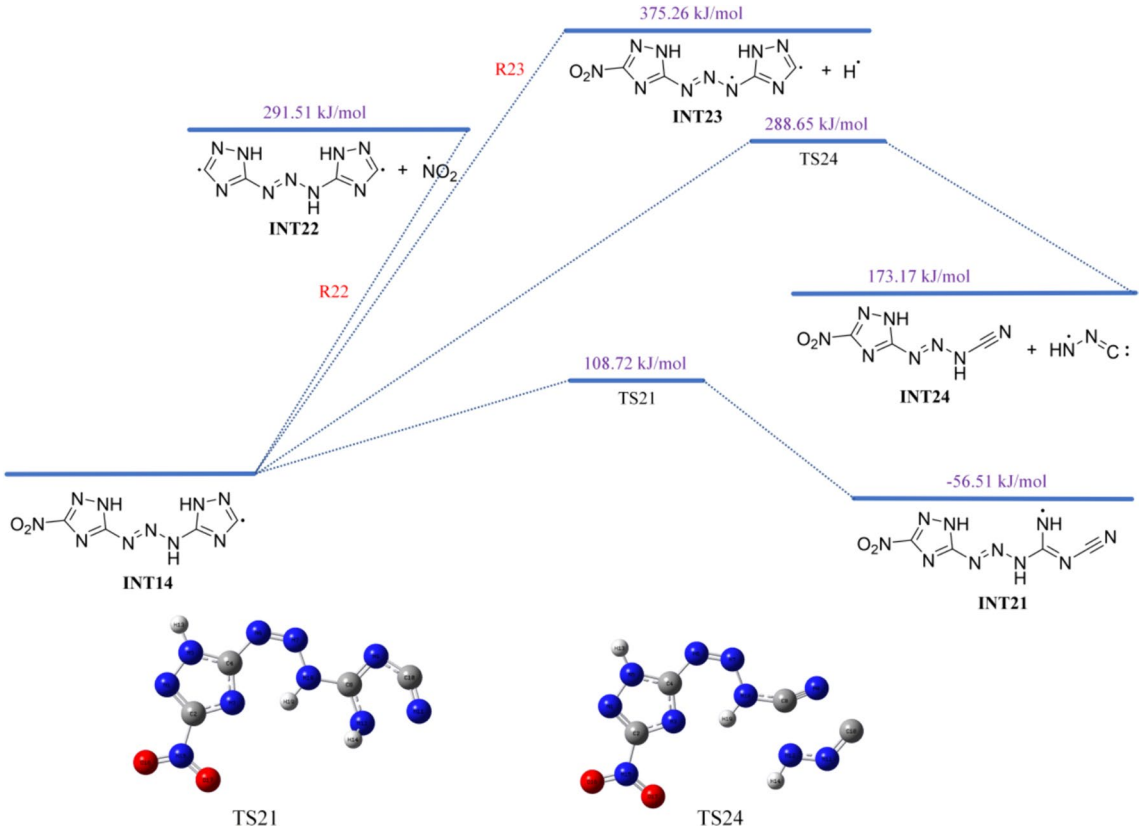

Fig. 3 Decomposition of **INT14** initiation reactions. All energy profiles (kJ/mol) show the relative Gibbs free energy with the energy of the initial reactant as zero

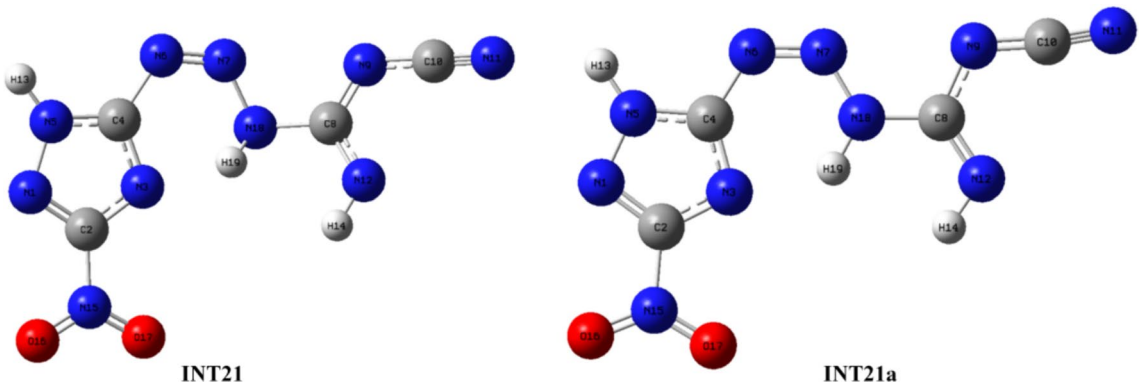

Fig. 4 Resonance isomers between **INT21** and **INT21a**

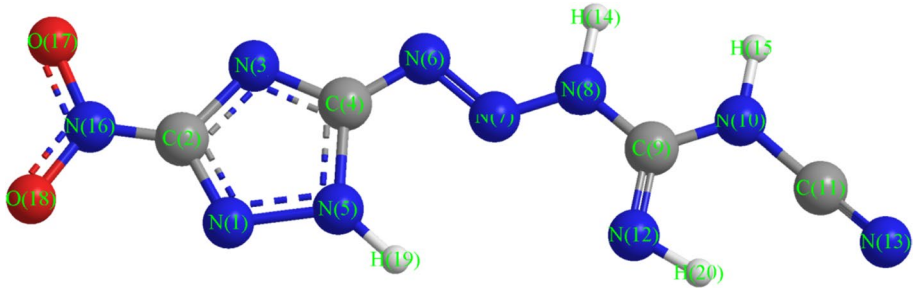

Fig. 5 Structure of *N*-cyano-3-(3-nitro-1*H*-1,2,4-triazol-5-yl) triaz-2-ene-1-carboximidamide

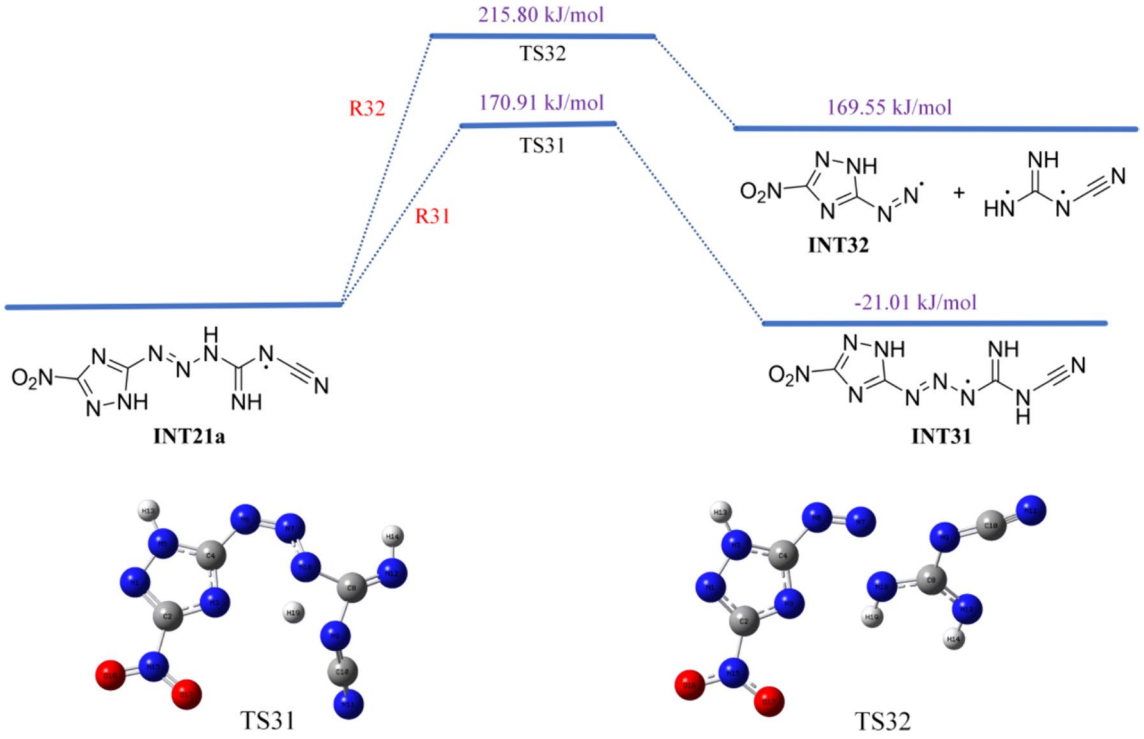

Fig. 6 Decomposition reactions of **INT21**. All energy profiles (kJ/mol) show the relative Gibbs free energy with the energy of the initial reactant as zero

breaking of single covalent bonds, one of their endothermicities was extremely large (> 450 kJ/mol). Since energies required for the homolytic dissociation of single covalent bond in **INT71** indicated that the rates for such reactions would be negligible at temperatures of interest, and suggesting that substances with conjugated double-bond structures are relatively stable. Other types of single covalent bonds were then investigated and might provide access to lower energy routes (see Fig. 9). The barrier of R71 was strongly lower than that of R73, producing cyanide radical and **INT73**. The nitro group of **INT61** was then eliminated via R72, whose barrier was 125.83 kJ/mol endothermic. A possible further decomposition step was characterized as R81 reaction process, but it was less favorable, as shown in Fig. 9.

3.4 Decomposition path of INT24

3.4.1 Initial decomposition of INT24

As a closed-shell intermediate, the energetically accessible paths for its unimolecular decomposition would be homolytic C–N (R33) or N–NH (R34) bond scission. As shown in Fig. 10, R33's endothermicity (205.21 kJ/mol) was slightly higher than that of R34 (204.37 kJ/mol), which were found to be almost identical. To our surprise, the formation of **INT33** is not the reaction of C–N cleavage and the retention of triazole ring. Hydrogen transfer and C=N bond cleavage are the key reactions, and formation of six-membered ring transition including C4–N3–H19–N18–N7–N6 atoms, which can be proved by the formation of transition state **TS33** (Fig. 10). Additionally, the old C4–N6, H19–N18, and C4–N3 bonds broke, and the new N3–H19 bond generated. At the same time, aromaticity of the triazole ring was destroyed, forming a five-membered heterocyclic ring with lone pair electrons **INT33**. Unlike the formation of **INT33**, **INT24** could fall apart to **INT32** and NHCN directly. Comparing these two decomposition processes, it was found that although the formation of **INT33** was at the expense of destroying aromaticity of the triazole ring, the formation of the six-membered ring transition state greatly weakens the barrier to the reaction and is more likely to occur.

3.4.2 Unimolecular decomposition of INT32

Postulating R52, R63, and R74 as a sequence of possible unimolecular steps for its decomposition, the homolytic breaking of single covalent bonds was identically low in their endothermicities. For the first step, with the cleavage of C–N bond, loss of small molecule nitrogen, and the formation of **INT52**, the reaction barrier of R52 is only 22.90 kJ/mol in a fairly exothermic step (− 5.92 kJ/mol). Secondly,

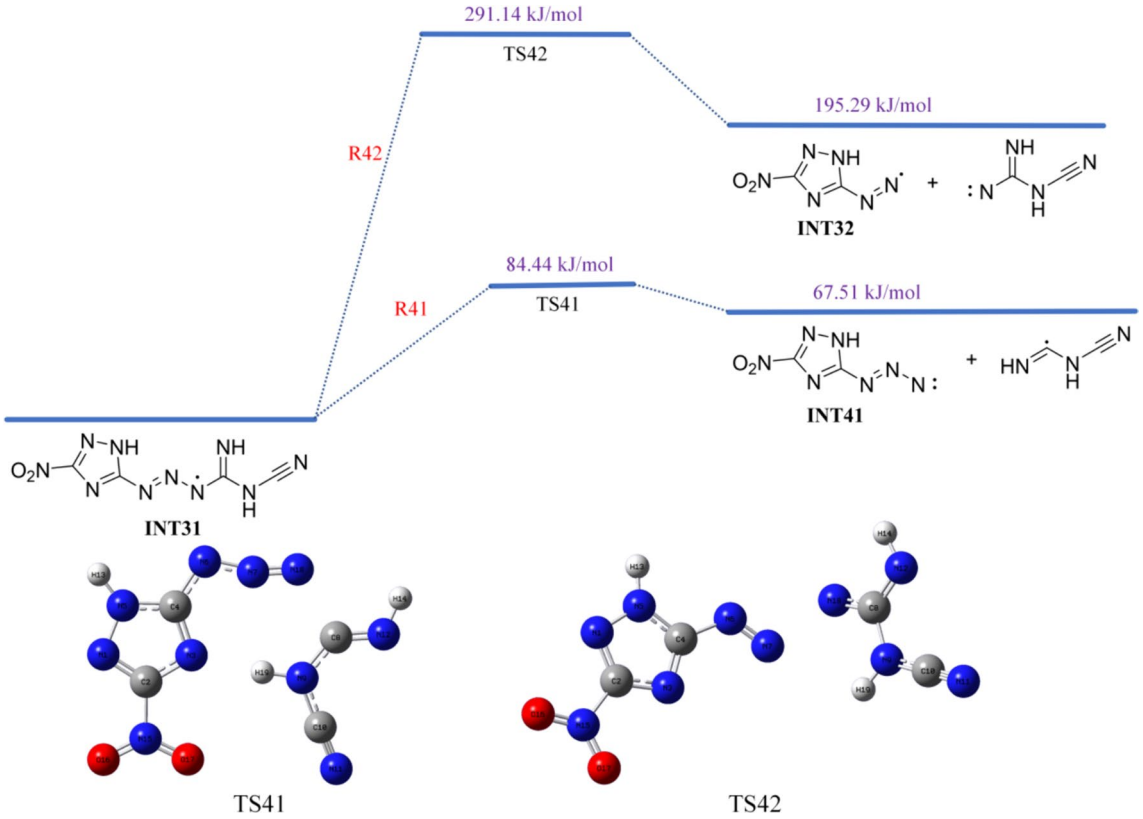

Fig. 7 Decomposition reactions of **INT31**. All energy profiles (kJ/mol) show the relative Gibbs free energy with the energy of the initial reactant as zero

after C–N bond cleavage of the triazole ring, its aromaticity disappeared, and R63 required a barrier of 181.11 kJ/mol, and an endothermicity of 93.27 kJ/mol.

The decomposition of **INT63** follows the principle of generating as many small molecule compounds as possible, and the breaking of N1–N5 bond allowed the formation of a free radical on either nitrogen atom, which can form two molecules CN–NO_2 and CN–NH eventually. This reaction should overcome a barrier of 69.77 kJ/mol to give **TS74** and an endothermicity of 38.86 kJ/mol (see Fig. 11).

It is concluded that energies required for the homolytic dissociation single covalent bonds in **INT32**, **INT52**, and **INT63** indicated that the rates for such reactions would be prefered at temperature of interest.

3.4.3 Unimolecular decomposition of INT33

INT33 is a kind of special structure, which has a carbon atom with a lone pair of electrons. Then, low-energy β-scission reactions were considered, radical **INT33** was postulated to decompose via the cleavage of N1–N5 and C2–N3 bonds. The barrier for R43 was found to be 160.47 kJ/mol, and the reaction was 35.65 kJ/mol endothermic (see Fig. 12), producing two closed-shell small molecules CN–NO_2 and NH=C=NH. Therefore, it would likely prove to be one of the favored routes.

In two cases, the unimolecular decompositions of **INT32** and **INT33** were close in energy barrier and products obtained, but different in decomposition steps. In view of the reasonable explanation of the above reaction process, both routes were speculated to be energetically favorable.

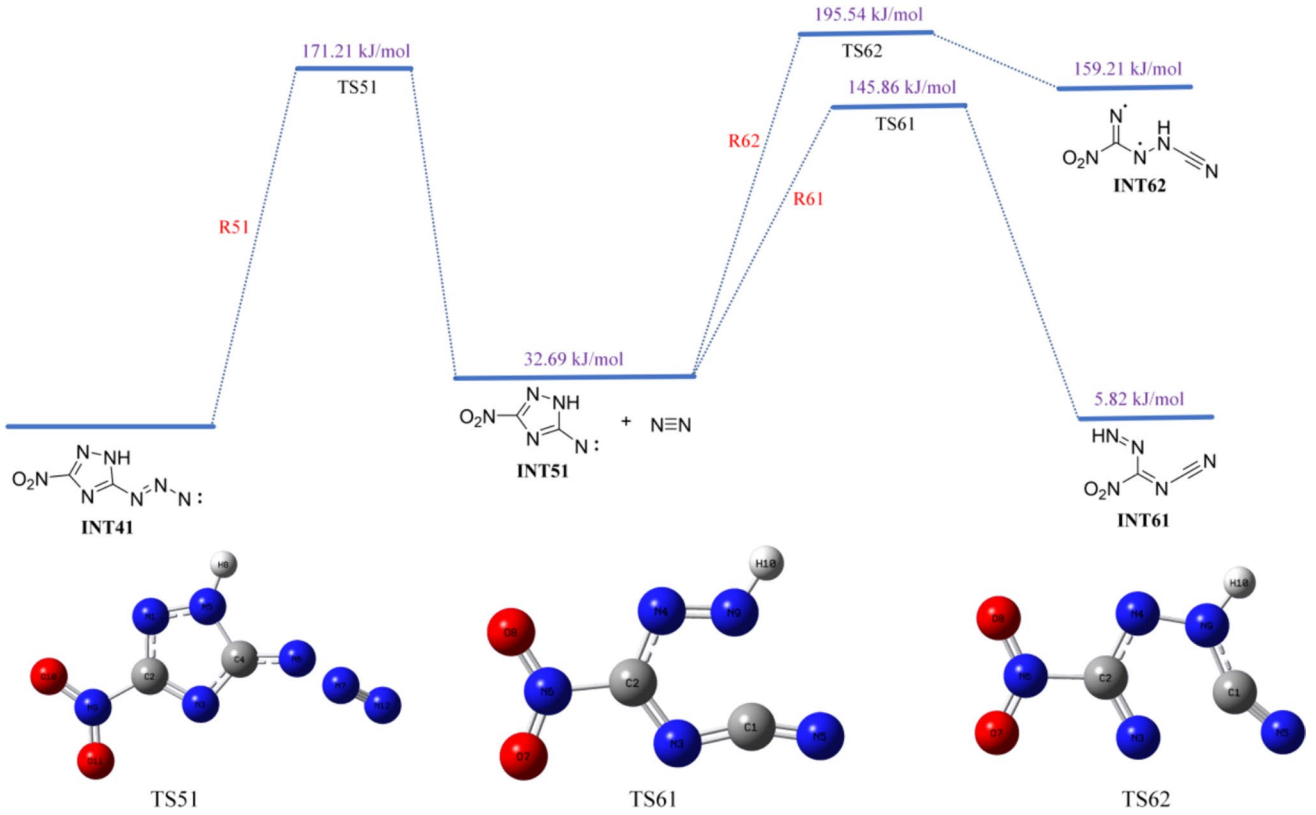

Fig. 8 Decomposition reactions of **INT41**. All energy profiles (kJ/mol) show the relative Gibbs free energy with the energy of the initial reactant as zero

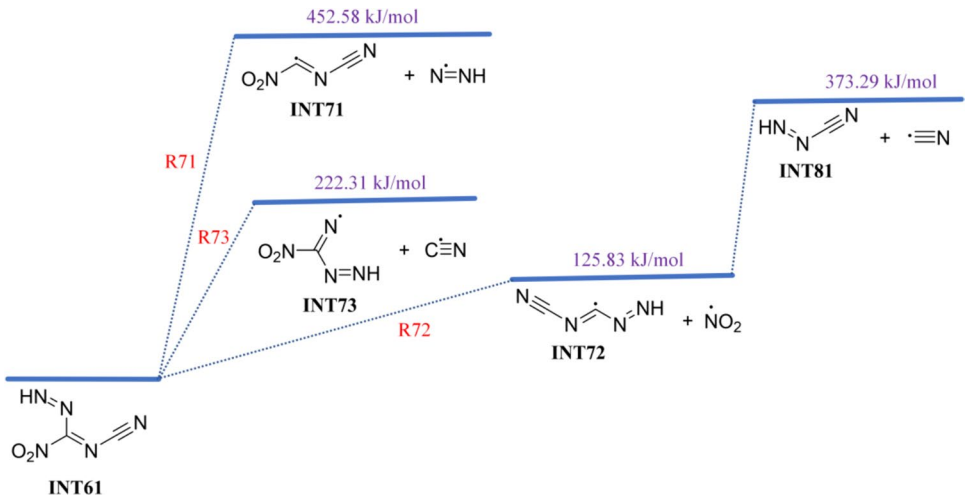

Fig. 9 Decomposition reactions of **INT61**. All energy profiles (kJ/mol) show the relative Gibbs free energy with the energy of the initial reactant as zero

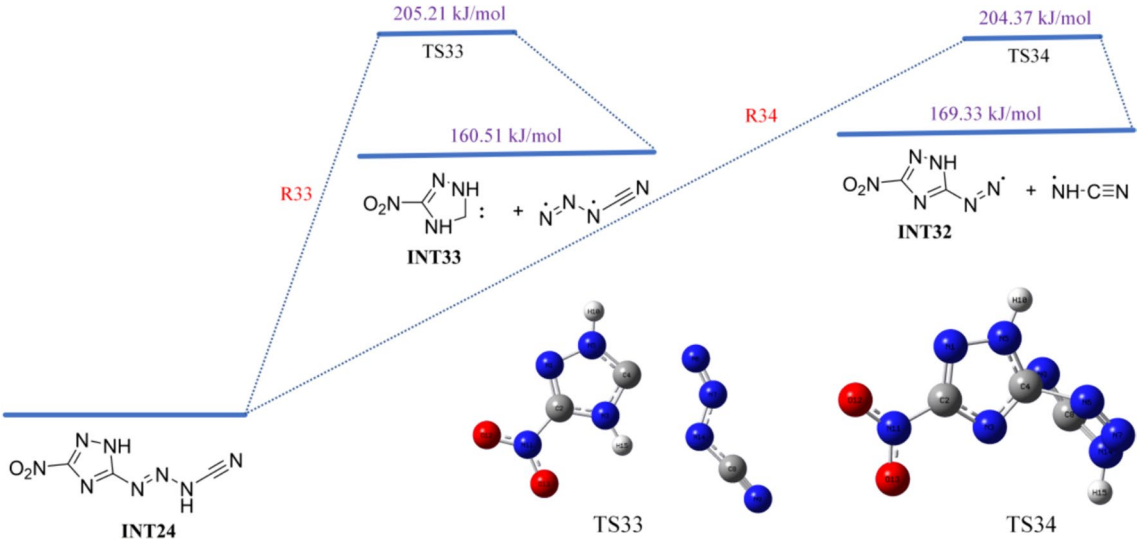

Fig. 10 Decomposition reactions of **INT24**. All energy profiles (kJ/mol) show the relative Gibbs free energy with the energy of the initial reactant as zero

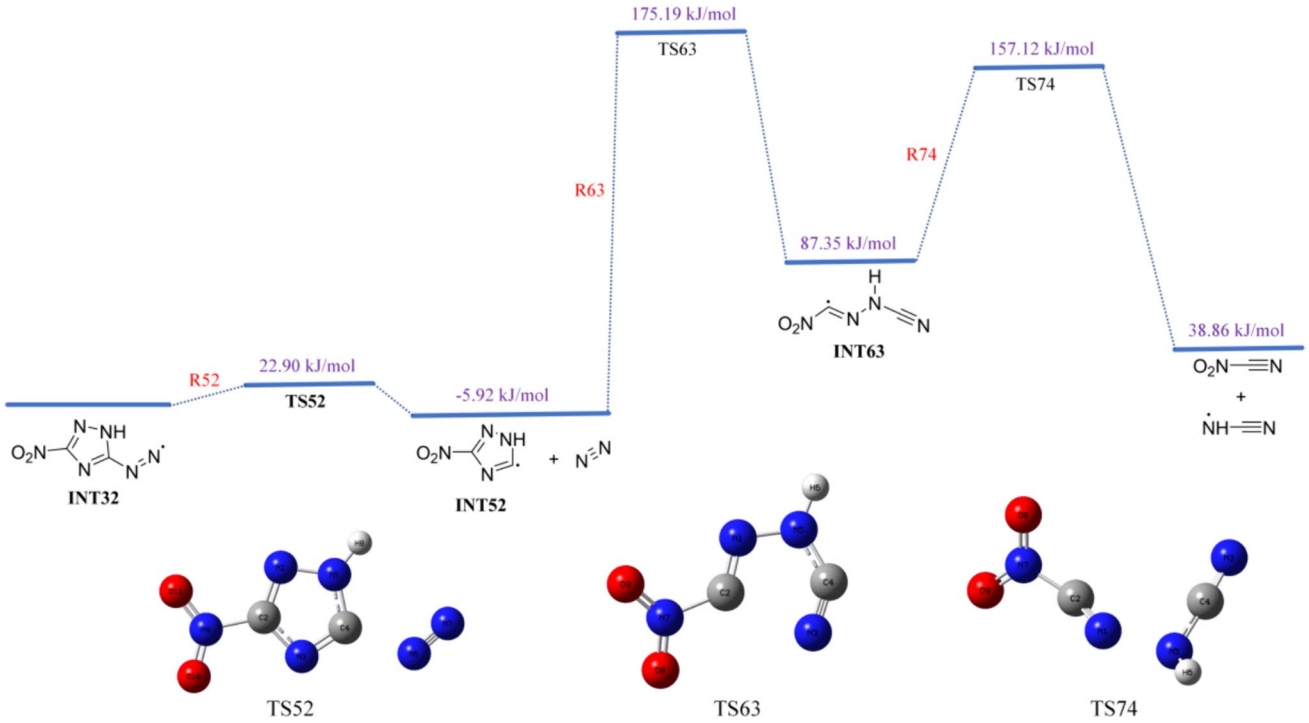

Fig. 11 Decomposition reactions of **INT32**. All energy profiles (kJ/mol) show the relative Gibbs free energy with the energy of the initial reactant as zero

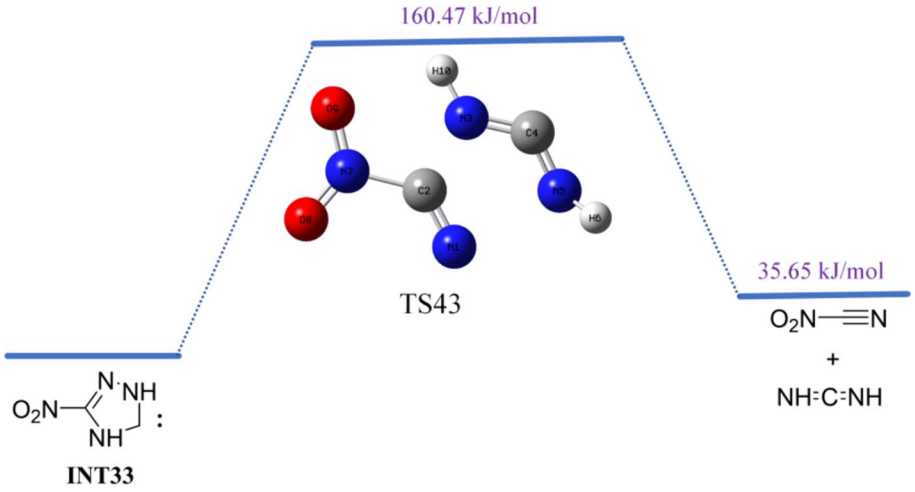

Fig. 12 Decomposition reactions of **INT33**. All energy profiles (kJ/mol) show the relative Gibbs free energy with the energy of the initial reactant as zero

4 Conclusions

Pathways for the thermal decomposition of **TBBT** were postulated and investigated with Gaussian using the M06-2× functional and the 6-311g(*d*,*p*) basis set. Particular attention was paid to unimolecular decomposition steps. *C*–NO_2 bond scission and ·NO_2 elimination are the primary dissociation pathway for **TBBT**, although the N–H bond holds a favorable position in LBO analysis. Besides, the reaction of breaking the N–N bond of the triazole ring to generate cyanide and NH radicals of **INT14** requires lower energy than the generation of cyanide and nitrotriazole linked to triazene, indicating that the decomposition product obtained is more stable when the free radicals formed after chemical bond cleavage have a tendency to form a chemical bond. The results also show that neutral molecules such as nitrogen and the formation of single free radicals such as nitro and cyanide groups are conducive to the generation of thermodynamically stable products.

Acknowledgements This research was supported by the Natural Science Foundation of Jiangsu Province (Grant No. BK20220352). We are so grateful to the High-Performance Computing Center of Nanjing Tech University for doing the numerical calculations in this paper on its x-Flex enterprise blade cluster system.

Author contributions Congming Ma helped in conceptualization, original draft, and funding acquisition. Kehan Hu contributed to writing—original draft. Peng Ma helped in methodology and supervision. Wenxin Xia contributed to writing—review and editing.

Data availability No datasets were generated or analysed during the current study.

Declarations

Conflict of interest On behalf of all authors, the corresponding author states that there is no conflict of interest.

References

1. Dippold AA, Klapötke TM (2013) A study of dinitro-bis-1,2,4-triazole-1,1′-diol and derivatives: design of high-performance insensitive energetic materials by the introduction of N-oxides. J Am Chem Soc 135:9931–9938. https://doi.org/10.1021/ja404164j
2. Thottempudi V, Shreeve JM (2011) Synthesis and promising properties of a new family of high-density energetic salts of 5-nitro-3-trinitromethyl-1*H*-1,2,4-triazole and 5,5′-bis(trinitromethyl)-3,3′-azo-1H-1,2,4-triazole. J Am Chem Soc 133:19982–19992. https://doi.org/10.1021/ja208990z
3. Zhang J, Dharavath S, Mitchell LA, Parrish DA, Shreeve JNM (2013) Energetic salts based on 3,5-bis(dinitromethyl)-1,2,4-triazole monoanion and dianion: controllable preparation, characterization, and high performance. J Am Chem Soc 138:7500–7503. https://doi.org/10.1021/jacs.6b03819
4. Klapötke TM, Minar NK, Stierstorfer J (2009) Investigations of bis (methyltetrazolyl) triazenes as nitrogen-rich ingredients in solid rocket propellants–synthesis, characterization and properties. Polyhedron 28(1):13–26. https://doi.org/10.1016/j.poly.2008.09.015
5. Feng S, Li F, Zhao X, Qian YD, Fei T, Yin P, Pang SP (2021) Comparative study on 1,2,3-triazole based azo-and triazene-bridged high-nitrogen energetic materials. Energ Mater Front 2:125–130. https://doi.org/10.1016/j.enmf.2021.03.006
6. Jiang X, Yang Y, Du H, Yang B, Tang P, Wu B, Ma C (2023) Triazene bridged energetic materials based on nitrotriazole: synthesis, characterization and laser ignited combustion performance. Dalton Trans 52:5226–5233. https://doi.org/10.1039/D2DT04007G
7. Jiang X, Li L, Yang Y, Du H, Wang Y, Zhu J, Ma C (2023) Boosting laser-ignited combustion performance of energetic materials with low sensitivity: integration of triazene-bridged triazole with oxygen-rich moieties via noncovalent self-assembly. Cryst Growth Des 23:333–341. https://doi.org/10.1021/acs.cgd.2c01039
8. Frisch MJ, Trucks GW, Schlegel HB, Scuseria GE, Robb MA, Cheeseman JR, Scalmani G, Barone V, Petersson GA, Nakatsuji H, Li X, Caricato M, Marenich AV, Bloino J, Janesko BG, Gomperts R, Mennucci B, Hratchian HP, Ortiz JV, Izmaylov AF, Sonnenberg JL, Williams Ding F, Lipparini F, Egidi F, Goings J, Peng B, Petrone A, Henderson T, Ranasinghe D, Zakrzewski VG, Gao J, Rega N, Zheng G, Liang W, Hada M, Ehara M, Toyota K,

Fukuda R, Hasegawa J, Ishida M, Nakajima T, Honda Y, Kitao O, Nakai H, Vreven T, Throssell K, Montgomery JA, Peralta JE, Ogliaro F, Bearpark MJ, Heyd JJ, Brothers EN, Kudin KN, Staroverov VN, Keith TA, Kobayashi R, Normand J, Raghavachari K, Rendell AP, Burant JC, Iyengar SS, Tomasi J, Cossi M, Millam JM, Klene M, Adamo C, Cammi R, Ochterski JW, Martin RL, Morokuma K, Farkas O, Foresman JB, Fox DJ (2016) Gaussian 16 Rev. C.01. Gaussian Inc., Wallingford

9. Lu T, Chen F (2012) Multiwfn: a multifunctional wavefunction analyzer. J Comput Chem 33:580–592. https://doi.org/10.1002/jcc.22885
10. Zhao Y, Truhlar DG (2008) The M06 suite of density functionals for main group thermochemistry, thermochemical kinetics, noncovalent interactions, excited states, and transition elements: two new functionals and systematic testing of four M06-class functionals and 12 other functionals. Theor Chem Acc 120:215–241. https://doi.org/10.1007/s00214-007-0310-x
11. Lu T, Chen Q (2021) Interaction region indicator: a simple real space function clearly revealing both chemical bonds and weak interactions. Chem Methods 1:231–239. https://doi.org/10.1002/cmtd.202100007
12. Veals JD, Chen CC (2021) Thermal decomposition of gas-phase bis(1,2,4-oxadiazole)bis(methylene) dinitrate (BODN): ACCSD(T)-F12/DFT-based study of reaction pathways. J Phys Chem A 125:9077–9091. https://doi.org/10.1021/acs.jpca.1c06065